IET Science, Measurement & Technology

Research Article

IET Journals
The Institution of Engineering and Technology

Investigation on Insulation Performance of Thermally Aged Natural Ester Oil Impregnated Pressboard

ISSN 1751-8822
Received on 13th March 2019
Revised 12th June 2019
Accepted on 31st July 2019
E-First on 2nd September 2019
doi: 10.1049/iet-smt.2019.0117
www.ietdl.org

Soumya Thakur[1], Ramanujam Sarathi[1] ✉

[1]*Department of Electrical Engineering, Indian Institute of Technology Madras, Chennai- 600036, India*

✉ *E-mail: rsarathi@iitm.ac.in*

Abstract: An attempt is made to understand the effect of thermal ageing on natural ester oil impregnated pressboard material. Surface discharge inception voltage of natural ester oil impregnated pressboard material is reduced drastically under AC, harmonic AC voltages and with DC voltages with high ripple content. Phase-resolved partial discharge studies show an increase in the number of discharges for natural ester oil impregnated pressboard (OIP) aged at higher temperature, under AC and harmonic AC voltages with different total harmonic distortions. Surface potential measurement study complies with results obtained by surface discharge inception voltage. It indicates the presence of high-density charge traps evolved as a function of ageing time and temperature. Laser-induced breakdown spectroscopy analysis is carried out to understand the characteristic variation with thermally aged OIP material. A decrease in plasma temperature is observed for sample aged at higher temperature. Differential scanning calorimetric studies indicate reduction in peak temperature with thermally aged specimens. Ageing observed to affect mechanical strength of the cellulosic material, as indicated by tensile test. Dielectric response spectroscopy study indicates that with an increase in thermal ageing, the permittivity, tan(δ), DC conductivity and relaxation time have increased. A reduction in activation energy of the aged material is observed, which indicates the status of the OIP material.

1 Introduction

Oil and the paper/pressboard materials are extensively used as an insulant in transformers. The failure of transformer during service conditions is closely associated with its insulation conditions and therefore it is of paramount importance to continuously monitor its status. In recent times, natural ester oil is gaining significant importance as a potential substitute of the conventional mineral oil insulation due to its higher dielectric strength, flash point, fire point, better resistance to moisture and oxidation, and its superior biodegradability compared to the latter [1]. Natural ester oil maintains higher breakdown voltage with large amount of dissolved water indicating higher tolerance to moisture ingress compared to mineral oil [2]. Despite higher affinity to oxidation and hydrolysis, ester oil shows better ageing stability compared to mineral oil. The investigations have shown that natural ester oil based cellulose insulation is found to retain considerable degree of polymerisation as compared to mineral oil, due to thermal ageing [3]. It is essential to understand the characteristic variation in OIP material due to thermal ageing in natural ester oil, particularly on exposure to different levels of thermal stress conditions.

The normal operating temperature of an oil-filled transformer lies around 60–65°C, but due to sudden increase in load current and intermittent faults; the transformer insulant temperature tends to increase. Mineral oils have poor heat transfer capabilities, which enhance localisation of heat at certain locations leading to local hotspot formation. The temperature at hotspots may rise to above 200°C which can adversely affect the pressboard insulation [4].

Converter transformers are one of the key components in high-voltage direct current (HVDC) transmission system, in which apart from thermal stress, the insulation is also subjected to electrical stress. The process of AC/DC conversion introduces distortion in output voltage waveform which reduces the voltage withstand capability due to the formation of harmonic voltage with different total harmonic distortions (THD) leading to high dv/dt stress. In an OIP specimen, pulsed DC have been reported to have a significant influence on partial discharge (PD) characteristics [5]. This necessitates the need to test the OIP material under possible cases of voltage waveform distortion. Conventionally discharge pattern recognition using phase-resolved partial discharge (PRPD) analysis is not possible for discharge occurring under DC supply, due to lack of periodicity. This has been overcome in the present work by analysis of ripple DC, which enables discharge pattern recognition and classification.

Conventional methods of identification of partial discharge formation is by periodic inspection of oil through dissolved gas analysis (DGA) (IEC 60567), moisture content (IEC 60814), furanic compounds (IEC 61198), which requires on-site examination. Thus identification of PD occurrences, using non-invasive ultra-high frequency (UHF) technique has gained considerable popularity owing to its high sensitivity and good signal-to-noise ratio [6]. In addition to electrical characterisation, optical signal analysis such as laser-induced breakdown spectroscopy (LIBS) is progressively used to estimate deposition of metal contaminants and the degradation status of insulation specimen [7]. Plasma generated by ablation of sample surface has been exploited in the current analysis to link it with the degradation status of insulation.

Thermal ageing can affect the dielectric properties of the material which can be monitored by analysing the frequency domain dielectric response. Several methods have been employed to analyse ageing condition of OIP for mineral oil based insulation using dielectric response studies. Similar analysis on understanding the variation in dielectric relaxation in thermally aged natural ester oil based OIP is scanty.

With the above overview of the literature, the present work is focused to investigate the characteristic variation of OIP due to thermal ageing. The study is broadly classified into three sections: (i) Understanding characteristic variations with thermally aged natural ester oil impregnated pressboard insulation through (a) surface discharge inception voltage (SDIV), (b) PRPD analysis and (c) surface potential measurement. (ii) LIBS analysis to sense and infer the plasma temperature and to obtain composition variation of thermally aged natural ester oil impregnated pressboard material and (iii) Physical parametric studies of thermally aged oil impregnated pressboard material using (a) DSC analysis, (b) tensile strength analysis and scanning electron microscopic image analysis (c) DRS studies and analysis of its different parameters using double relaxation model of OIP aged specimens under different thermal stress.

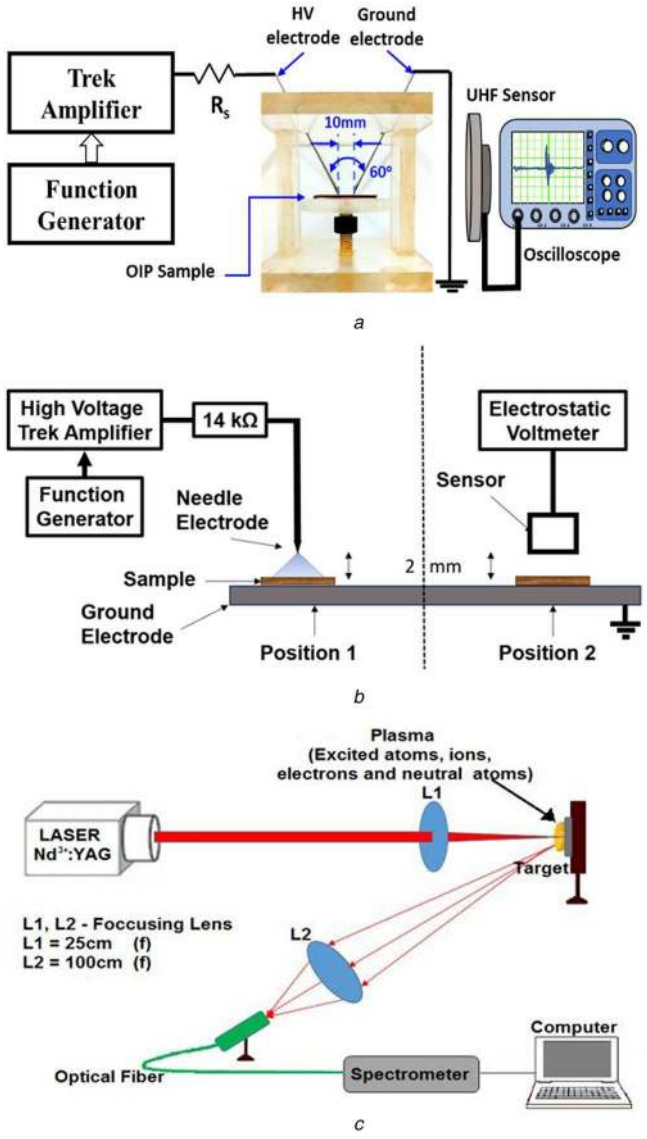

Fig. 1 *Experimental setup for*
(a) Surface discharge inception voltage analysis, ***(b)*** Surface potential measurement, ***(c)*** Laser-induced breakdown spectroscopy

2 Experimental setups

2.1 Thermal ageing

To understand the effect of thermal degradation of transformer insulation, accelerated thermal ageing studies were carried out with MIDEL 1204 Rapeseed natural ester oil with pressboard material (commercially procured from Andrew Yule Pvt. Ltd.). Table 1 shows the initial physicochemical parameters of rapeseed ester oil and OIP used in current analysis.

The pressboard material is heated in air circulated oven at 120°C for 4 h, to remove any moisture content in it, after which is subjected to impregnation. Impregnation of cellulosic OIP specimen is carried out to remove all air cavities from the cellulosic fiber structure such that occurrence of partial discharges can be avoided and uniform dielectric properties can be achieved. Rate of impregnation in ester oil is reported to be comparable to mineral oil impregnation at temperature raised up to three times [8]. At elevated temperatures oil viscosity reduces enhancing its capillary action, but on further increasing the temperature surface tension of the oil is compromised. Thus, in the present study 6 h time duration was fixed for impregnation of OIP, carried out at 70°C with the height of oil and OIP stack maintained at 20 and 10 mm, respectively.

The maximum limit of ageing temperature given by IEEE standards for acceptance and maintenance of natural ester fluids in transformers is 180°C, to avoid fluid scorching such that the watt density does not exceed 2 W cm^{-2} (12 W in^{-2}) [9]. Thus, the maximum thermal stress subjected in the current study is limited to 180°C. Thermal ageing studies were carried out at three different temperatures which include: 70°C, 140°C and 180°C for 500 h in a temperature-controlled thermostat. To provide near condition, as in a transformer, the pressboard material wrapped with copper material and oil was kept in the weight ratio of 1:1:10. OIP material of 2 mm thickness wrapped with a thin copper sheet of 0.5 mm thickness are kept with 1 L of natural ester oil, in which nitrogen ambience is maintained at a constant pressure to avoid oxidation. After removal, the OIP samples are cleaned with acetone to remove oil and kept in a desiccator for further analysis. The OIP aged at 70°C, 140°C and 180°C are referred to as sample A, sample B and sample C, respectively.

Table 1 Initial properties of rapeseed ester oil and pressboard used in present analysis

Natural ester oil characteristics		Pressboard characteristics	
density (at room temperature) (g/m^3)	0.92	density (g/cm^3)	1.2
dissipation factor (at 90°C) (tan delta)	<0.03	dissipation factor (at 30°C, 50 Hz) (tan delta)	0.3
water content	50	permittivity (at 30°C, 50 Hz)	5
dielectric breakdown (kV/mm)	45	thickness (mm)	2
acid number	0.04		

2.2 Experimental setup for surface discharge studies

Fig. 1*a* shows the experimental setup for understanding the surface-discharge characteristics of OIP material. Test conditions are chosen to reproducibly and conveniently accelerate a process of simulating surface discharge activity. The electrode setup used for analysing surface discharge studies is adopted as per the IEC 60112 standard. The high voltage and ground electrode are symmetrically arranged such that the total angle between them is 60° and with opposite electrode tips lie approximately on the flat horizontal surface of the OIP specimen. The electrode end is chisel-edged at 30° angle with radius 0.1 mm [10]. The electrode configuration is selected such that large electric field gradient is induced at the tip of the conductor enhancing tangential electric field over the sample surface. A series resistor (R_s) of 10 MΩ is included in the circuit to limit the leakage current.

The high voltage applied across the electrode is generated using a function generator (Tektronix AFG3051C 5GSa/s, 50 MHz). The output of the function generator is fed to a high voltage trek amplifier which amplifies the input signal by a factor of 6000. The voltage applied to the test setup to the required level, at a rate of 300 V/s.

In order to generate harmonics induced sinusoidal voltage and ripple-induced direct voltage, input to function generator is modified. THD present in the harmonic AC voltage waveform is calculated as

$$\mathrm{THD} = \frac{\sqrt{V_2^2 + V_3^2 + V_4^2 + \cdots + V_n^2}}{V_1} \quad (1)$$

where V_n is the rms voltage magnitudes of the nth harmonic and $n = 1$ is the fundamental frequency of the supply voltage. In the current analysis, third, fifth and seventh harmonic voltages are superimposed on fundamental sinusoidal voltage in order to generate the output voltage with desired %THD. The THD is varied up to 20% to consider the possibility of distortion reported in converter-type transformers.

For generating AC voltage of desired THD content with harmonics of 3ω, 5ω, 7ω where $\omega = 2\pi \times 50$ Hz, the following equation were employed:

$$V(t) = V_s(\sin\omega t + 0.01h\sin(n\omega t)) \quad (2)$$

$$\text{Crest factor(CF)} = V_p/V_{rms} \quad (3)$$

$$\text{Form factor(FF)} = V_{rms}/V_{avg} \quad (4)$$

With suitable values of harmonic n and percentage h, it is possible to generate the desired harmonic AC voltage with required THDs.

For generating ripple DC output, a simplistic full wave rectifier output of a three-phase supply is computed and fed to the function generator. The ripple percentage (r%) is calculated as the ratio of peak to peak value of ripple (V_{rp-p}) in the output and the expected mean value of dc voltage (V) as given by (2)

$$r\% = \frac{V_{rp-p}}{V} \times 100 \quad (5)$$

The non-directional UHF sensor is kept at a distance of 20 cm, to avoid any flashover between the test cell and the sensor. The output probe of the UHF sensor is connected to a digital storage oscilloscope which records data at a sampling rate of 40 GSa/s.

2.3 Surface potential measurement

The experimental setup used in the present study for surface potential measurement is shown in Fig. 1*b*. Conventionally, three different techniques are used to inject charges to an insulating material: sharp point emitter, corona discharge process and external corona source. The charges injected get accumulated on the surface of the insulating material, and may even get trapped in voids or other defective zones of the material. The resistivity of the material determines the magnitude of the charge deposition. The presence of these charges is reflected in the form of potential build-up on the surface.

In the present analysis, a needle plane configuration was used for the generation of corona. The top needle electrode is connected to the high voltage and the plane electrode is connected to the ground electrode. The radius of curvature of the high voltage needle electrode is 50 µm. The sample surface on which the charge needs to be deposited is placed over the ground electrode. The supply voltage for generating corona activity was maintained at 12 kV DC, generated using Trek amplifier. After a specific time, duration (5 min) of charging, the charged specimen is shifted to position 2 where the surface potential is measured using an electrostatic voltmeter (Trek Model 341B). A gap distance of 2 mm is maintained between the sensor and the test specimen. Thus, two stages are involved in surface potential measurement of the specimen. In the first stage, the charge is deposited (referred to as position-1) by corona discharge process. After a given time period, the sample is moved on the same platform to position-2 and surface potential was measured using an electrostatic voltmeter.

2.4 Laser induced breakdown spectroscopy

LIBS study was carried out by irradiating the OIP surface by a nanosecond pulsed laser (Nd^{3+}: YAG laser, (Minilite II, Continuum) of wavelength 1064 nm, energy 10 mJ). Fig. 1*c* shows LIBS setup. The Nd^{3+}YAG laser is focused on the sample using a lens with focal length 25 mm. The optical emission is captured with the help of a 100 cm focal length lens and is passed to a spectrometer (ocean optics) through an optical fibre of core diameter 400 µm, 0.22 numerical aperture (NA). The emitted plasma is focused on an optical fibre receiver (core diameter 600 µm, 0.39 NA) by another lens of 150 mm focal length. The fibre coupled spectrometer (MCS FLEX PDA, UV-NIR, Tec5 AG) enables to record and analyze data. In order to reduce the interference from continuum radiation in the characteristic signal emissions, an appropriate triggering delay was applied to the spectrometer.

2.5 Frequency domain dielectric response spectroscopy

The dielectric response of OIP material was obtained by using Novo control technology broadband dielectric/impedance spectrometer (Alpha – a high-performance frequency analyser).

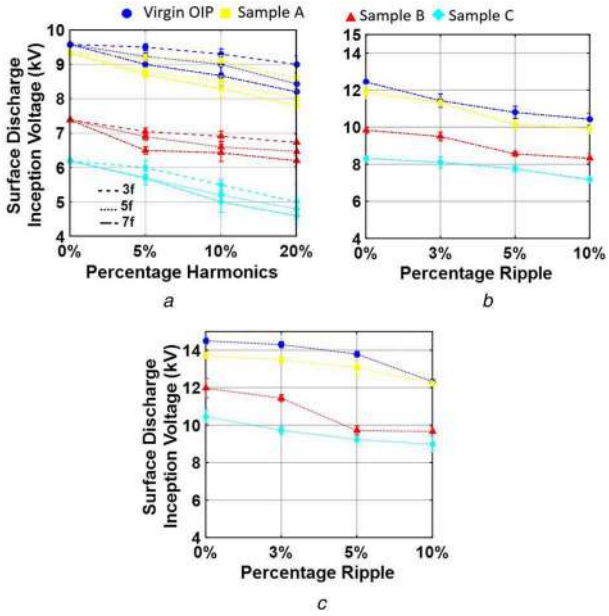

Fig. 2 *Surface discharge inception voltage of virgin and aged OIP samples at different temperatures on application of*
(a) Pure sinusoidal and harmonic induced AC voltages, ***(b)*** Positive, ***(c)*** Negative DC voltage with different percentage of ripple

The dielectric constant and the dielectric loss measurements were carried out in the range of 10^{-2}–10^{6} Hz, at temperatures ranging 30–90°C.

3 Results and discussions

3.1 Surface discharge inception voltage analysis adopting UHF technique

Fig. 2 shows the variation in SDIV of natural ester oil impregnated pressboard material under AC and DC voltages. The SDIV value obtained is an average of 25 readings and the standard deviation obtained is much lower than 3% and hence the average value is indicated. Increase in ageing temperature showed reduced SDIV of natural ester oil impregnated pressboard material, under AC and DC voltages. This can be explained as at higher ageing temperatures, the rate of carbonisation of fibre and cleavage of covalent bonds in cellulose accelerates leading to the formation of low molecular weight organic molecules and acidic residues [11]. The acidic residues enhance the conductivity and the cleaved bonds enhances charge trap site enhancing the tangential electric field to initiate surface discharge activity at lower voltages.

Thermal ageing of ester oil leads to a reduction in ester content and enhancement in acidic residue in oil. It is reported that upon thermal ageing, ester gets transformed to propyl linoleate and carboxylic acids, including hexadecanoic acid and octadecanoic acid [11]. These acidic residues aids in loosening of tight cellulosic hydrogen bond network resulting in formation of low molecular weight compounds. During thermal degradation, molecular level changes take place in oil; homolytic cleavage of carbon–carbon or carbon–hydrogen bond takes place. Smaller free radicals (like hydrogen, methyl, and ethyl) are relatively stable; larger free radicals break down to form smaller, more stable radicals and other unsaturated olefin compounds. The free radicals are reactive and they undergo chain reactions to form lighter lower boiling unsaturated compounds, gases and additional free radicals [12]. The organic acids and water formed as a by-product of ageing are highly bipolar in nature and thus leads in enhancement of conductivity along with increase in hydrogen ion concentration in the insulation. The presence of acidic residues enhance the polarisation and depolarisation current in the OIP. This could be explained as thermal ageing leads to production of ions formed due to dissociation of ageing by-products [13].

In Fig. 2*a*, it is observed that on application of AC voltage, irrespective of the sample, the presence of harmonics degrades the

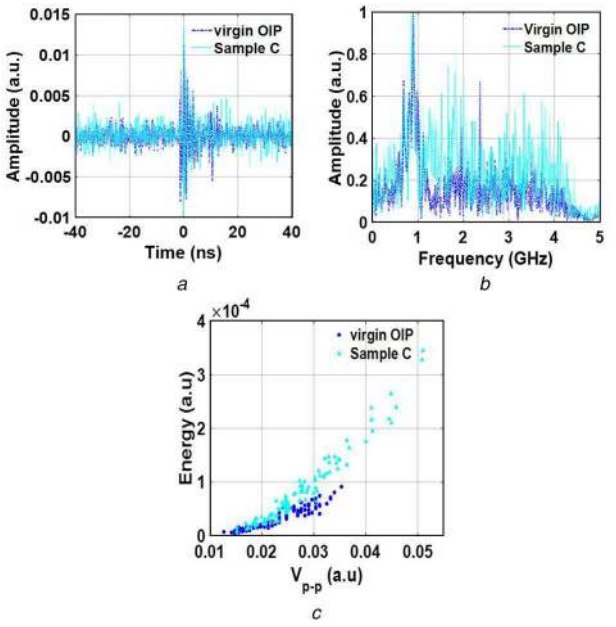

Fig. 3 *UHF signal analysis*
(a) Typical UHF signal formed due to surface discharge activity, ***(b)*** FFT of the UHF signals captured, ***(c)*** Energy vs peak to peak analysis of UHF signal obtained for a sequence data collected for virgin and aged OIP sample

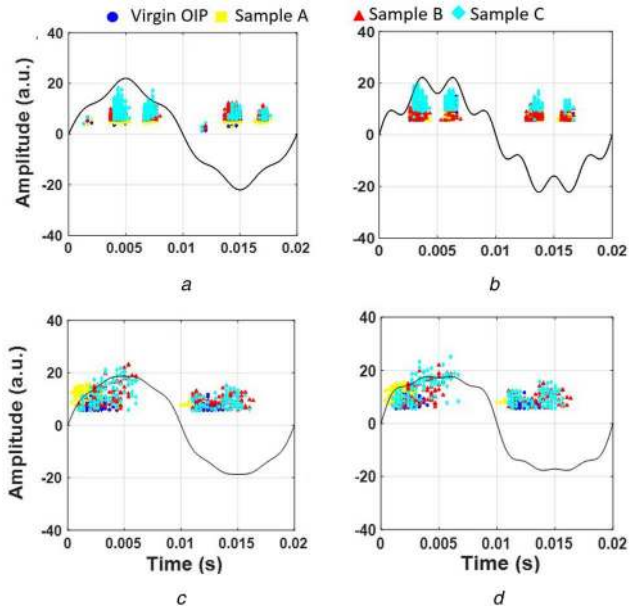

Fig. 4 *PRPD plots of thermally aged OIP samples under harmonic AC voltages with different THDs*
(a) 10% THD of 5f, ***(b)*** 20% THD of 7f, ***(c)*** 10% THD of 3f + 5f + 7f harmonics, ***(d)*** 20% THD of 3f + 5f + 7f harmonics

SDIV, this degradation is more when the %THD and frequency content of harmonics is increased. Dao and Phung [14] have reported that the presence of waveform distortion adversely affects the reliability and life of insulation.

Figs. 2*b* and *c* show the influence of ripple content in positive and negative DC voltage on SDIV with natural ester oil impregnated pressboard material respectively. A marginal reduction in SDIV is observed with an increase in ripple content in DC voltages. Surface discharge is often correlated to the charge deposited on the surface layer of the insulation. Surface discharge initiates with field emission of electrons from cathode triple junction (interface point of electrode, insulator surface and ambient air), which is followed by secondary electron emission [15]. Compared to AC voltage, the OIP has higher SDIV under DC voltages. Among DC voltage, positive DC voltage has lower SDIV than under negative DC voltages.

Beroual and Khaled [16] have studied surface discharge activity and have indicated that for a given voltage, the final discharge length is high under AC voltage and the least under negative DC voltage. Du *et al.* [17] have indicated that charge trapping is high under negative polarity than the positive polarity and the positive charge gets discharged quickly. Linhjell *et al*. [18] have indicated that the formation of positive streamer occurs at much lower voltage than in the case of negative streamers. On application of high voltage to the electrode gap, injected charges get trapped into the oil impregnated pressboard material. In the process, at the triplet junction, surface discharge activity gets initiated [19]. In the process, the positive trapped charges could aid the increment of oil pressboard interface electric field initiating the surface discharge process. Under negative polarity, due to lower discharge length and lower dissipation rate of trapped negative charges, the surface discharge process gets mitigated and higher voltage is required to move the trapped charges aiding the surface discharge activity.

Since pulsation of DC is a result of AC component of multiple frequencies, the discharge pattern follows a trend similar to that under AC voltage application. The increase of percentage ripple has a similar impact as with harmonic voltage with higher THDs.

Fig. 3*a* shows the typical UHF signal formed due to surface discharge activity with virgin and thermally aged OIP sample. It is observed from FFT analysis (Fig. 3*b*) that UHF signal detected has its dominant frequency near 1 GHz. The UHF signal obtained is related to surface discharge magnitude, as the energy of the signal is directly proportional to q^2 [6]. Fig. 3*c* shows energy analysis of 100 UHF signals, taken in sequence mode at inception voltage, where energy is calculated as

$$E_i = \frac{\sum_i v_i^2}{R_L} \tag{6}$$

where v_i is signal amplitude and R_L is the cable impedance (50 Ω). Compared to virgin OIP the energy of discharge signals increases for the thermally aged specimen. Though thermal ageing at elevated temperature leads to gradual desorption of moisture content already existing in the pressboard, the percentage moisture content in aged OIP sample is reported to enhance [1]. The increase in PD signal can be attributed to the enhanced moisture content in cellulosic structure due to accelerated ageing or could be due to acidic residue and bond breakage of cellulose, which acts as a charge trap site. The water content in aged OIP may be formed by external inflow or from pyrolysis (oxidative degradation) of the pressboard. Lelekakis *et al.* [20] have described oxidative degradation reaction on primary and secondary alcohol groups (–OH) of the cellulose chain, which forms aldhehydes, ketones, carboxylic acids, thus opening the glucose ring and disrupting the cellulose chain. These reactions create water permitting hydrolysis of the cellulose. The generated water molecules react with the highly hydrophilic hydroxyl groups of cellulose structure and results into subsequent breakdown of inter-polymer hydrogen bonds and result into loss of mechanical strength.

3.2 Phase-resolved partial discharge analysis

Phase-resolved partial discharge (PRPD) analysis was carried out by connecting the UHF sensor to the spectrum analyser and operated in zero span mode with central frequency same as the dominant frequency of 1 GHz generated due to surface discharge activity (Fig. 3*b*). The output of the function generator used for applying voltage across the test cell is synchronised with the spectrum analyser, to relate the discharge with the phase of occurance.

Fig. 4 shows the PRPD analysis obtained during surface discharge activity under AC with harmonic AC voltages with different THDs. It is observed that surface discharge occurs near the zero crossing of the AC voltage waveform in both positive and negative cycles. This property of surface discharge helps distinguish it from other types of incipient discharge. Under harmonic AC voltage, the concentration of discharges occurs where dv/dt stress is high. It is observed that the discharge phase window and the number of discharges are seen to increase

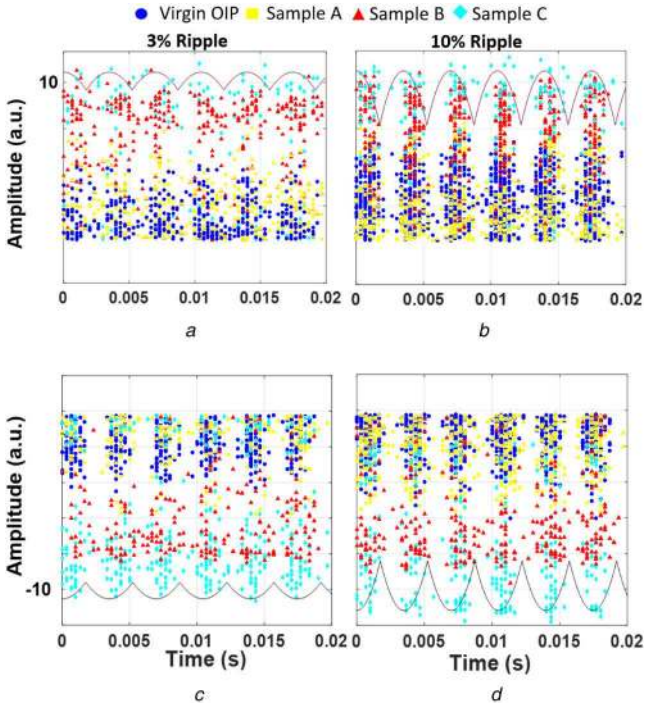

Fig. 5 *PRPD plots of thermally aged OIP samples under DC voltages with different percentage of ripple contents*
(a) 3%, ***(b)*** 10% positive DC ripple, ***(c)*** 3%, ***(d)*** 10% negative DC ripple

proportionally with THD, frequency content of harmonics and ageing temperature. Effect of mixed frequency harmonics voltages (Figs. 4*c–d*) results in discharges of much higher magnitude over a longer time window. Sample A and virgin OIP exhibit similar characteristics, whereas samples B and C have higher discharge magnitude. This can be explained as a result of surface charge traps on OIP which leads to increment in the tangential electric field allowing high magnitude discharges with an increase in thermal ageing temperature [21].

In HVDC system, distortion is found to be in DC voltage due to the presence of ripple. In the valve side of converter transformers, the insulation endures a composite voltage of AC harmonics and DC pulses. These ripples are periodic and thus helps to overcome the shortcoming of using PRPD analysis for DC voltage stress. Dezenzo *et al.* [5, 22] have carried out PRPD analysis of positive and negative ripple on needle plane configuration and reported that at high voltage, discharge magnitude follows inverse of the voltage curve due to the presence of dominant space charge. Fig. 5 shows the discharge pattern under different ripple DC application for surface discharge activity with OIP samples. It is observed that under DC voltage with higher ripple contents, discharges tend to occur at the slope of the ripples in both positive and negative DC voltage application. Number of discharges are more with negative DC voltage than with ripple compared to positive DC and AC voltage. In general, it is observed that for thermally aged specimen the surface discharge activity is high.

3.3 Surface potential measurement

The surface potential study can help one to understand the impact of thermal ageing on level of the degradation of cellulose surface. The understanding of surface potential measurement with natural ester oil impregnated pressboard material is scanty. Fig. 6*a* shows characteristic variation in surface potential on deposition of charge by corona charging. On removal of surface charging, surface potential exhibits an exponential decay. This decay can be characterised mathematically as

$$V(t) = V_o \mathrm{e}^{-t/\tau} \tag{7}$$

where V_o is the initial surface potential and τ as the decay time constant.

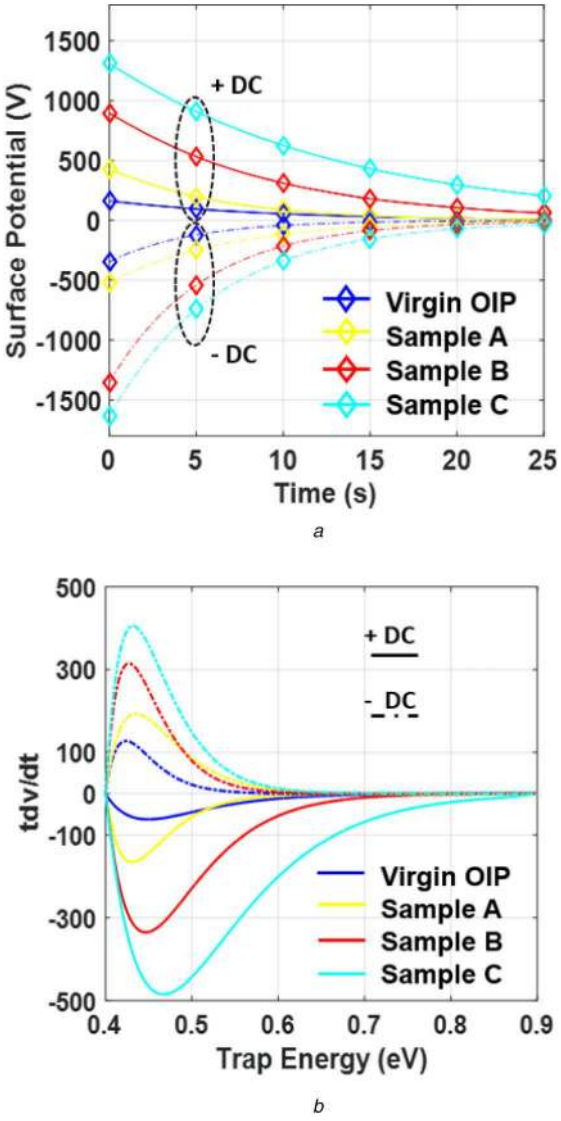

Fig. 6 *Surface Potential Analysis for OIP Samples*
(a) Surface potential decay characteristics of thermally aged natural ester oil impregnated pressboard material, under positive and negative DC voltages, ***(b)*** Corresponding trap energy characteristics for different OIP samples

It is interesting to note that though initial potential stored is observed to be more for negative DC supply charged OIP, the decay rate is less for positive polarity. This could be understood as negative charge tends to accumulate faster than positive charges in pressboard material. It is observed that compared to virgin sample where the effect is negligible, aged sample shows a considerable increase in surface potential. Sample C shows maximum initial surface potential followed with sample B, sample A and virgin OIP sample. This indicates the direct impact of ageing temperature on charge trap density on the surface of OIP material.

Level of damage of OIP material due to thermal stress can be further understood by analysing trap density calculated using Simmons and Tam's theory. Table 2 provides initial potential, the decay time constant and trap density (10^{-38} eV^{-1} m^{-3}). The potential decay graph can be utilised for obtaining the trap density and energy associated with it. The trap density and energy associated with it calculated as [23]

$$N_{\mathrm{t}}(E) = \frac{4\varepsilon_0\varepsilon_{\mathrm{r}}}{eL^2kT}\left|t\frac{\mathrm{d}V_s(t)}{\mathrm{d}t}\right| \tag{8}$$

$$E_{\mathrm{t}} = kTln(vt) \tag{9}$$

where N_{t} is the trap density in eV^{-1} m^{-3}, E is the trap energy in eV, ε_0 is the absolute and ε_{r} is the relative permittivity of material, e is

Table 2 Initial potential measured and their corresponding time decays and trap density for different thermally aged pressboard specimen

Sample type	ε_r	+DC supply			−DC supply		
		V_o (V)	τ(s)	trap density (N_t)	$-V_o$, V	τ(s)	trap density (N_t)
virgin OIP	7.0	163	3.09	0.0058	345	2.1	0.0019
sample A	8.2	427	3.12	0.0181	514	2.17	0.0088
Sample B	8.9	895	4.44	1.5428	1353	2.91	0.5909
sample C	13.6	1309	6.25	3.3282	1631	4.08	1.0984

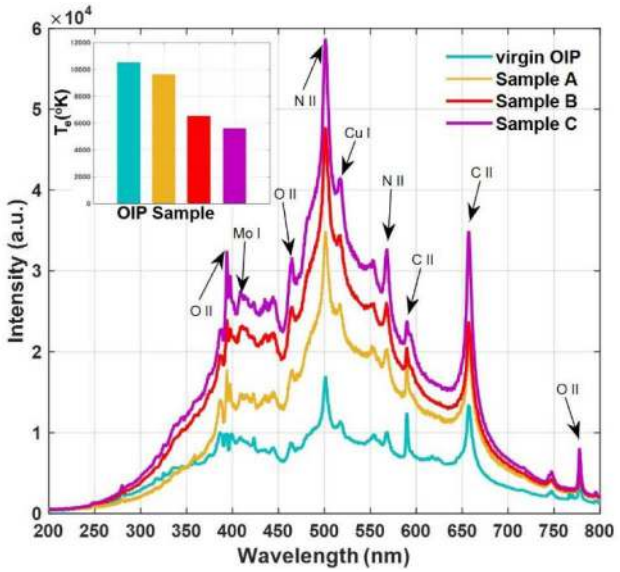

Fig. 7 *LIBS spectra of virgin and thermally aged natural ester oil impregnated pressboard materials*

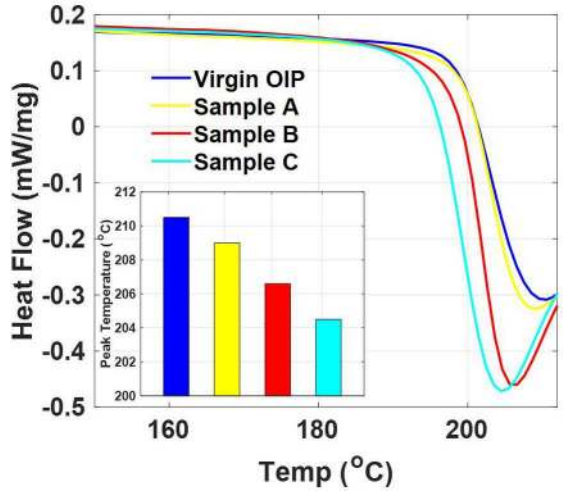

Fig. 8 *DSC analysis for thermally aged natural ester OIP samples*

the electron charge in Coulombs, L is the material thickness in meters, k (J/K) is the Boltzmann constant, T is temperature in Kelvin, v is the attempt to escape frequency in Hz (s^{-1}) and V_s is the voltage as a function of time t (s).

The rate of potential decay as a function of trap energy is given in Fig. 6*b*. The peaks in the figure are indicative of charge traps induced on the OIP surface as the trap density is directly proportional to tdv/dt. The trapping and de-trapping are associated with charge transfer capacity, deeper the charge trap, lower the decay rate, indicating charges will take more time to escape. In the present analysis, it is observed that deeper traps are formed with positive polarity charge injection than under negative polarity DC voltage. Du *et al.* [17] have reported that for OIP samples, positive DC tends to have more charges trapping tendency than negative DC. Also, the depth is more for OIP aged at higher temperature. This characteristic is observed irrespective of the polarity of voltage application. Also, it is observed that there exists a linear relationship between potential decay time constant and trap density. Increased trap density upon exposure to higher thermal stress could be attributed to the formation of new charge storing sites formed due to an increase in moisture content of OIP with ageing.

3.4 Laser-induced breakdown spectroscopy

LIBS has evolved as an effective method for characterising ageing and the decomposition level with transformer insulation [7]. Fig. 7 shows the LIBS graph obtained for different natural ester oil impregnated pressboard samples. It can be observed that with ageing the intensity of the signal obtained increases. The various peaks obtained are indicative of elements present in discharge plasma and can be identified by comparing by NIST database [24]. Carbon, oxygen and copper are among the predominant peaks. OIP is essentially a cellulosic structure composed of long hydrocarbon chains. When kept in the test setup and exposed to thermal stress, these chains tend to break leading to the easy escape of electrons and the formation of higher temperature of plasma as indicated by Fig. 7. The plasma temperature is calculated using Boltzmann–Saha equation with the assumption of local thermal equilibrium [25]

$$T_e = 1.44\frac{E_2 - E_1}{\ln[(I_1\lambda_1 A_2 g_2)/(I_2\lambda_2 A_1 g_1)]} \tag{10}$$

where excited energy levels are given by E_1 and E_2, statistical weights of excited energy levels 1 and 2 are denoted by g_1 and g_2 are, respectively, transition probabilities of states by A_1 and A_2, respectively, at wavelengths, λ_1 and λ_2, I_1 and I_2 are intensities of particular atomic species, respectively, and T_e is the plasma electron temperature assuming of local thermodynamic equilibrium. The plasma temperature is calculated for carbon peaks in the spectrum obtained. The T_e is found to be higher for virgin sample followed by samples A, B and C (Fig. 7). The irradiation of plasma for aged cellulose sample at lower temperatures could be attributed to its chemical decomposition where long polymeric chains of cellulose converts into furanose isomers, anhydrous sugar and low molecular weight oxygenates [11]. The decrease in temperature of plasma generated upon ablation of surface by laser is linked with the surface recession. Thus, the level of degradation of OIP material could be characterised for its ageing condition and performance, adopting LIBS.

3.5 Differential scanning calorimetry

The reduced irradiation plasma temperature observed in LIBS analysis can be understood by obtaining DSC analysis of OIP. As shown in Fig. 8, the peak temperature of dissociation of cellulose decreases from virgin OIP to sample C, aged at the highest temperature. The reduction of peak temperature with OIP sample aged at higher temperature can be attributed to breakage of hydroxyl and glycosidic bonds in the molecular chain of OIP which affects the micromorphology of the fibre surface, reducing intermolecular and intramolecular forces [26].

Peak temperature is indicative of onset of oxidative degradation of the sample. A reduction in peak temperature for sample C indicates the reduction in the thermal stability with ageing, which can be directly related to the reduced lifetime of OIP insulation. Polansky *et al.* [27] have correlated DSC results with tanδ values

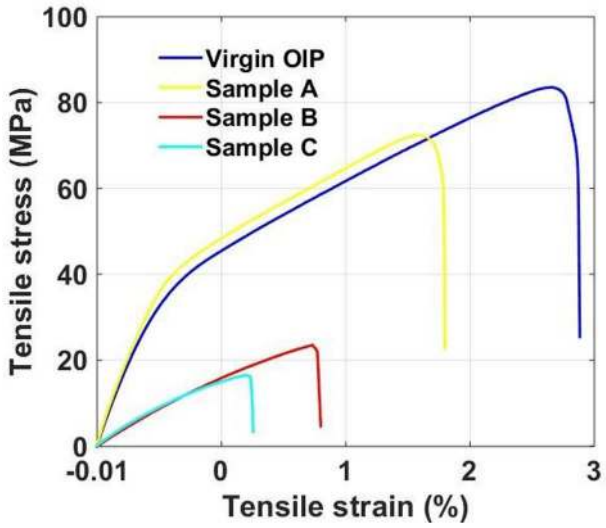

Fig. 9 *Stress–strain relationship for thermally aged natural ester OIP samples*

and have reported their efficiency in determining the degradation state and end of lifetime of transformer insulation.

3.6 Tensile strength and scanning electron microscopic image analysis for aged OIP material

Fig. 9 shows the tensile strength of the thermally aged ester oil impregnated pressboard material. It is observed that ageing temperature hase a high impact on tensile strength, with ageing at a higher temperature, OIP tends to become more brittle. Liao *et al.* [28] have observed that with ageing hydrogen bonds between OIP fibres brake reducing the crystallinity of structure non-linearly, making it brittle. The surface of OIP contains highly hydrophilic hydroxyl groups, which aids the breakage of inter-polymer hydrogen bonds, resulting in loss of mechanical strength [29]. Reduced tensile strength is indicative of cellulosic scission of bonds leading to a site for charge trap sites which could be realised based on the reduction in SDIV, trap depth of the material and with reduced plasma temperature.

Fig. 10 shows typical scanning electron microscopy (SEM) image obtained for virgin and aged OIP sample. Virgin sample is observed to have well-packed dense interwoven fiber network. Thermal degradation leads to fiber delamination which deteriorates cellulose structure. Liao *et al.*, have reported thinning of fiber structure as a consequence of ageing which is attributed to scission of hydrogen bond chains between the fiber structure [28]. OIP aged at higher temperature exhibits cracks in fiber structure and the formation of holes and punctures, which in turn acts as charge trapping sites. This is in well correlation with results obtained in surface potential measurements (Fig. 6).

3.7 Dielectric response spectroscopy

Dielectric response of OIP insulation has been investigated to get information regarding the impact of ageing. Linhjell *et al.* [30] have used dielectric response analysis for estimating moisture and low molecular weight acids in mineral OIP. They have emphasised the need to investigate validity of results for estimating ageing status of OIP. The molecular relaxation process gets altered based upon the characteristic variation in OIP sample. Dielectric relaxation analysis can help in understanding these variations which can explain the reduction in dielectric strength and increment in dielectric losses with thermal ageing.

Figs. 11*a* and *b* show variation in permittivity and loss factor of thermally aged OIP material. The measurements were carried out at different temperatures ranging from 30 to 90°C. It has been observed that with the increase in ageing temperature, both ε' and ε'' increases. The variation in values is more significant at lower frequency as at the lower frequency dipole movement is obstructed and hence relaxation time is more.

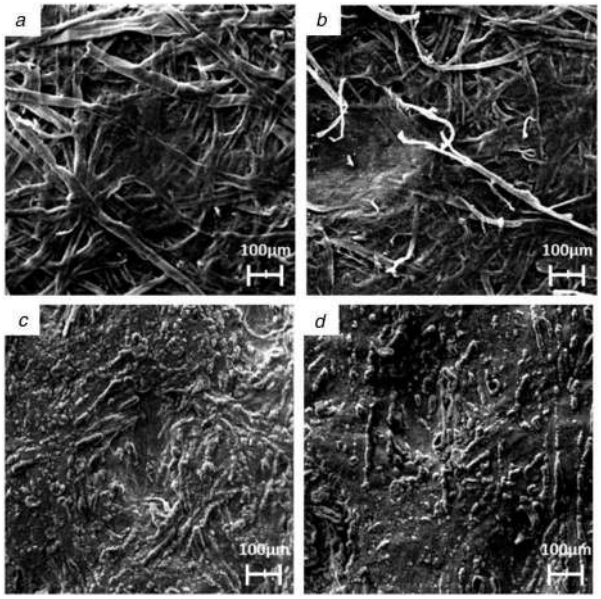

Fig. 10 *SEM images of*
(a) Virgin and OIP samples aged at, ***(b)*** 70°C, ***(c)*** 140°C, ***(d)*** 180°C

Fig. 11*c* shows the variation in dissipation factor (tan δ) with thermally aged natural ester oil impregnated pressboard material. tan δ is observed to be more for the sample aged at a higher temperature and seems to increase as the measuring temperature increases. This can be explained as the increase in ester oil conductivity, reduction in the degree of polymerisation value of OIP and enhancement of relaxation of polarisation at higher temperature [31].The process of polarisation and depolarisation on the application of alternating voltage follow the ac cycle and relaxation process. For a complex dielectric like OIP, more than a single relaxation time may exist owing to its complex molecular structure [32]. Bandara *et al.* [31] have reported the presence of multiple relaxation peaks for pressboard samples and have concluded that the relaxation process at higher frequency is affected by moisture content in the OIP. Conventional Debye equation does not sufficiently describe the experimental results as it does not account for non-exponential relaxation laws. In the present analysis for relating the dielectric properties with relaxation time Cole–Cole double relaxation has been used [33]. In the present study, ε' is related to frequency by inverse power law and time constants are estimated by Cole–Cole expressions with τ_1 and τ_2 as two relaxation time given by

$$\varepsilon' = A\omega^{-n} + \mathrm{Re}\left(\frac{\Delta\varepsilon_1}{1+(j\omega\tau_1)^{1-\alpha_1}} + \frac{\Delta\varepsilon_2}{1+(j\omega\tau_2)^{1-\alpha_2}}\right) \tag{11}$$

$$\varepsilon'' = \frac{\sigma_{\mathrm{dc}}}{\omega\varepsilon_o} + A\omega^{-n}\cot\left(\frac{(1-n)\pi}{2}\right) + \mathrm{Im}\left(\frac{\Delta\varepsilon_1}{1+(j\omega\tau_1)^{1-\alpha_1}} + \frac{\Delta\varepsilon_2}{1+(j\omega\tau_2)^{1-\alpha_2}}\right) \tag{12}$$

For estimating imaginary part, ε'' Kramers–Kronig (K-K) transformation is used by using least-mean square error to estimate the parameters [34]. A represents the intensity of low-frequency dispersion and ω is the frequency in radians ω, n is a constant and σ_{dc} is the DC conductivity. Change in permittivity of the first and second Cole–Cole process are represented by $\Delta\varepsilon_1$ and $\Delta\varepsilon_2$, respectively. The two processes of Cole–Cole relaxation at lower and higher frequencies are represented by the two terms, respectively, ε_∞ that is the value of permittivity at the infinite frequency is assumed as 1, α_1 and α_2 are coefficients of Cole–Cole relaxation times.

The initial parameters in each case are adjusted to minimise the mean square error. The modelled values of the real and imaginary part of permittivity are represented for 90°C as shown by markers

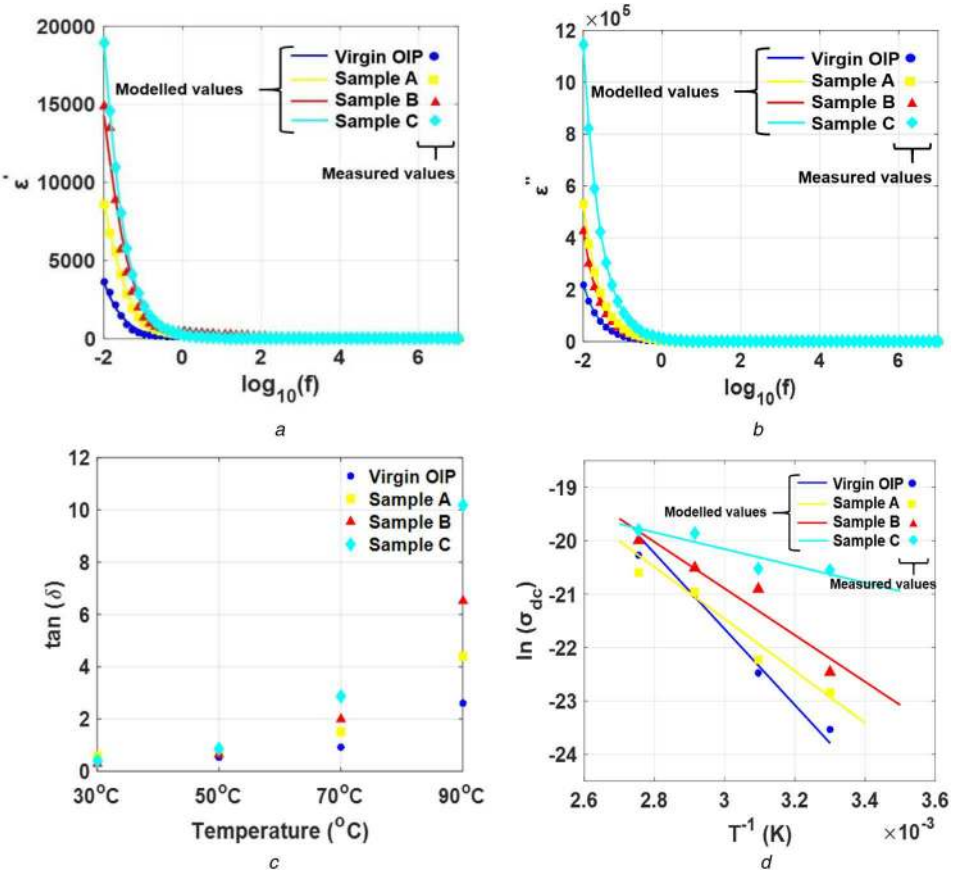

Fig. 11 *Dielectric Response Analysis*

(a) Real and, ***(b)*** Imaginary permittivity values measured and modelled for aged OIP samples at 90°C, ***(c)*** Dielectric loss (tan δ) of different OIP samples at different temperatures of measurement, ***(d)*** Arrhenius plot for dc conductivity for different samples as a function of measuring temperature

Table 3 Estimated model parameters of dielectric constant of OIP sample at different measurement temperatures

$P \downarrow T$ (°C→)	Virgin OIP				Sample A				Sample B				Sample C			
	30	**50**	**70**	**90**	**30**	**50**	**70**	**90**	**30**	**50**	**70**	**90**	**30**	**50**	**70**	**90**
A	3.10	17.4	32.6	122	18.0	19.2	44.8	204	21	37.0	102	317	35.5	108	493	706
N	0.03	0.04	0.19	0.57	0.12	0.06	0.16	0.17	0.21	0.96	1.64	1.08	0.11	0.43	0.97	0.23
$\Delta\varepsilon_1 \times 10^2$	0.62	2.00	15.0	69.2	30.2	2.69	118	43.6	30.0	17.5	84.4	223	288	80.8	165	44.2
$\tau_1 \times 10^3$	6.16	6.04	5.94	5.75	6.18	5.98	5.9	5.52	6.1	6.32	5.31	3.01	2.07	6.46	2.17	1.06
α_1	0.29	0.26	6.71	2.41	0.22	0.35	0.01	0.02	0.22	0.15	0.04	0.18	0.53	0.02	0.05	0.53
$\Delta\varepsilon_2 \times 10^2$	0.11	26.0	29.4	191	3.45	18.1	11.9	38.5	3.8	38.1	460	11.4	483	79.2	6.80	84.6
$\tau_2 \times 10^{-6}$	17.6	15.1	12.6	7.31	12.5	12.1	11.8	6.6	11.5	9.7	9.6	4.1	4.13	2.39	1.88	1.43
α_2	0.06	1.61	0.12	0.01	3.08	5.29	0.02	7.25	0.47	3.18	3.08	7.01	0.01	0.60	7.17	0.03
$\sigma_{dc} \times 10^{-11}$	5.98	17.3	75.1	157	12.1	22.2	78.9	113	17.4	82.9	124	208	119	123	235	249
$E_a \times 10^4$	5.912				4.047				3.628				1.306			

Bold values indicate the bold font in table are specifying the parameters calculated.

in Figs. 11*a* and *b*. The modelled parameter exhibits a close correlation with the measured values. Similar estimation is carried out for all the samples at all temperatures of measurement. The values of constants for the final fitted graph are encapsulated in Table 3, where P indicates the different parameter and T is measurement temperature.

It can be inferred from the values of Table 3 that accelerated ageing at high temperatures decrease the relaxation time (τ_1, τ_2) of dielectric material. Irrespective of the type of sample, the time constants decrease with increase in measuring temperature. This can be explained as higher temperature enhances the mobility of dipoles which results in smaller relaxation time. Here τ_1, τ_2 represents the first- and second-relaxation process occurring at lower and higher frequencies, resectively. Compared to second-relaxation process, dielectric parameters are more pronounced in first. This is evdent from the higher variation in parameters (A, n, $\Delta\varepsilon_1$, α_1, τ_1) at lower frequency range compared to high frequency (α_2, $\Delta\varepsilon_2$ and τ_2). Another important observation is dependence of dc conductivity on ageing temperature. The conductivity can be visualised as a consequence of motion of charges, enhancing the conduction current and polarisation in the dielectric; thus contributing to the dielectric loss. This correlates the increase in conductivity value with increase in dielectric loss value as shown in Fig. 11*a*. These values of relaxation time and dc conductivity can be used to estimate dielectric degradation condition in practical applications.

The above suggested model gives dc conductivity by relating ε' and ε'' equations. These values can be related to temperature using Arrhenius relationship

$$\sigma_{dc} = Ae^{-E_a/RT} \quad (13)$$

where A is a pre-exponential constant, R is the universal gas constant, T is temperature in Kelvin and E_a represents the activation energy in J/mol Fig. 11d shows variation of activation energy, calculated as the slope of linear fit of σ_{dc} as a function of temperature. These slopes can be extrapolated to find conductivity at other temperatures. It is realised that activation energy thus calculated is direct indication of degradation of OIP stresses under thermal ageing (Table 3). Thus, it can be used as a fingerprint to determine end of life criteria for cellulosic insulation used in a natural ester oil filled transformer.

4 Conclusions

The present investigation aimed at understanding the impact of different thermal stress intensities on natural ester oil based OIP specimen.

Effect of thermal ageing on surface properties of natural ester OIP is characterised using surface potential decay and SDIV analysis. Results indicate that for samples aged at a higher temperature, the initial potential and decay time constant of surface potential is higher for sample aged at at higher temperature, which indicates trapping of charges at the surface of OIP for more thermally degraded sample and is also reflected in the trap energy and density measurements. This was accompanied by a reduction in SDIV of aged OIP sample characterised using UHF analysis. With thermal ageing of OIP specimen, energy of the UHF signal. This was further investigated by the results of PRPD analysis which marked that surface discharge activity occurs at zero crossing of the signal and the number of discharges increases with thermally aged OIP material. Also, the number of discharges due to surface discharge activity enhances under harmonic AC voltages and with increase in ripple content in the DC voltage supply, which could possibly explain the reduction in SDIV for higher percentage THD of AC harmonics and percentage ripple of DC supply voltage.

Optical analysis using LIBS revealed a reduction in plasma temperature with thermally aged specimens indicating the presence of surface recession. DSC studies clearly indicate a reduction in peak temperature indicating reduced thermal stability of more thermally degraded OIP specimen. A reduction in tensile strength has been observed with thermally aged OIP material which could be attributed to fibre delamination as seen by SEM analysis. DRS study indicates that with thermal ageing of natural ester OIP material degrades it dielectric properties. The permittivity, tan(δ), DC conductivity and relaxation time are observed to increase for aged OIP. Also, a reduction in activation energy of the thermally aged material was observed, which explains the physicochemical degradation of aged OIP.

5 Acknowledgment

The authors wish to thank CPRI, Bangalore for extending the test facilities obtained for the sponsored NPP project to IIT Madras.

6 References

[1] Martin, D., Saha, T., McPherson, L.: 'Condition monitoring of vegetable oil insulation in in-service power transformers: some data spanning 10 years', *IEEE Electr. Insul. Mag.*, 2017, **33**, (2), pp. 44–51

[2] CIGRE: 'Brochure of CIGRE No 436, experiences in service with new insulating liquids', 2010

[3] Coulibaly, M.L., Perrier, C., Marugan, M., *et al.*: 'Aging behavior of cellulosic materials in presence of mineral oil and ester liquids under various conditions', *IEEE Trans. Dielectr. Electr. Insul.*, 2013, **20**, (6), pp. 1971–1976

[4] Hamdi, A., Fofana, I., Djillali, M.: 'Stability of mineral oil and oil–ester mixtures under thermal ageing and electrical discharges', *IET Gener. Transm. Distrib.*, 2017, **11**, (9), pp. 2384–2392

[5] Dezenzo, T., Betz, T., Schwarzbacher, A., *et al.*: 'The different stages of PRPD pattern for positive point to plane corona driven by a DC voltage containing ripple', *IEEE Trans. Dielectr. Electr. Insul. Vol.*, 2018, **25**, (1), pp. 30–37

[6] Judd, M.D., Cleary, G.P.: 'UHF and current pulse measurements of partial discharge activity in mineral oil', *IEE Proc. Sci. Meas. Technol.*, 2006, **153**, (2), pp. 47–54

[7] Lin, Z., Han, W., Xiao, H., *et al.*: 'Study of silicone rubber used at external insulation of high voltage with laser-induced breakdown spectroscopy (LIBS)'. 2016 IEEE Int. Power Modulator and High Voltage Conf., IPMHVC 2016, San Francisco, USA, 2017, pp. 671–674

[8] Dai, J., Wang, Z.D.: 'A comparison of the impregnation of cellulose insulation by ester and mineral oil', *IEEE Trans. Dielectr. Electr. Insul.*, 2008, **15**, (2), pp. 374–380

[9] IEEE Std C57.147TM: 'IEEE std c57.147^{TM}-2011-guide for acceptance and maintenance of natural ester fluids in transformers', 2008

[10] IEC-60112: 'International standard', *Int. Organ.*, 2003, **1**, pp. 15–19

[11] Thakur, S., Sarathi, R., Gautam, R., *et al.*: 'Thermal aging of cellulosic pressboard material and its surface discharge and chemical characterization', *Cellulose*, 2017, **24**, (11), pp. 5197–5210

[12] Kongbonga, Y.G.M., Ghalila, H., Onana, M.B., *et al.*: 'Characterization of vegetable oils by fluorescence spectroscopy', *Food Nutr. Sci.*, 2011, **2**, (7), pp. 692–699

[13] Koch, M., Tenbohlen, S.: 'Diagnostics of oil-paper-insulations using relaxation currents', 14th Int. symp. High Voltage, Beijing China, 2005, pp. 507–512

[14] Dao, T., Phung, B.T.: 'Effects of voltage harmonic on losses and temperature rise in distribution transformers', *IET Gener. Transm. Distrib.*, 2017, **12**, (2), pp. 347–354

[15] Anderson, R.A., Brainard, J.P.: 'Mechanism of pulsed surface flashover involving electron-stimulated desorption', *J. Appl. Phys.*, 1980, **51**, (3), pp. 1414–1421

[16] Beroual, A., Khaled, U.: 'Influence of hydrostatic pressure on creeping discharge characteristics over solid/liquid insulating interfaces under AC and DC voltages', *IET Gener. Transm. Distrib.*, 2017, **12**, (2), pp. 267–271

[17] Du, B.X., Jiang, J.P., Zhang, J.G., *et al.*: 'Dynamic behavior of surface charge on double-layer oil–paper insulation under pulse voltage', *IEEE Trans. Dielectr. Electr. Insul.*, 2016, **23**, (5), pp. 2712–2719

[18] Linhjell, D., Lundgaard, L., Berg, G.: 'Streamer propagation under impulse voltage in long point-plane oil gaps', *IEEE Trans. Dielectr. Electr. Insul.*, 1994, **1**, (3), pp. 447–458

[19] Zainuddin, H., Mitchinson, P.M., Lewin, P.L.: 'A method for the measurement of leakage current due to surface discharge at the oil-pressboard interface'. 2011 Electrical Insulation Conf., EIC 2011, Annapolis, USA, 2011, pp. 41–44

[20] Lelekakis, N., Martin, D., Wijaya, J.: 'Ageing rate of paper insulation used in power transformers part 2: oil/paper system with medium and high oxygen concentration', *IEEE Trans. Dielectr. Electr. Insul.*, 2012, **19**, (6), pp. 2009–2018

[21] Mitchinson, P.M., Lewin, P.L., Strawbridge, B.D., *et al.*: 'Tracking and surface discharge at the oilpressboard interface', *IEEE Electr. Insul. Mag.*, 2010, **26**, (2), pp. 35–41

[22] Dezenzo, T., Betz, T., Schwarzbacher, A., *et al.*: 'The different stages of PRPD pattern for negative point to plane corona driven by a DC voltage containing a ripple', *IEEE Trans. Dielectr. Electr. Insul.*, 2017, **24**, (1), pp. 47–53

[23] Simmons, J.G., Tam, M.C.: 'Theory of isothermal currents and the direct determination of trap parameters in semiconductors and insulators containing arbitrary trap distributions', *Phys. Rev. B*, 1973, **7**, (8), pp. 3706–3713

[24] Sansonetti, J.E., Martin, W.C.: 'Handbook of basic atomic spectroscopic data', *J. Phys. Chem. Ref. Data*, 2005, **34**, (4), pp. 1559–2259

[25] Descoeudres, A., Hollenstein, C., Demellayer, R., *et al.*: 'Optical emission spectroscopy of electrical discharge machining plasma', *J. Mater. Process. Technol.*, 2004, **149**, pp. 184–190

[26] Wang, Y., Wang, Y., Jiang, X.: 'The microscopic morphology of insulation pressboard: an image processing perspective', *Cellulose*, 2018, **25**, (5), pp. 3051–3065

[27] Polansky, R., Prosr, P., Vik, R., *et al.*: 'Comparison of the mineral oil lifetime estimates obtained by differential scanning calorimetry, infrared spectroscopy, and dielectric dissipation factor measurements', *Thermochim. Acta*, 2017, **647**, pp. 86–93

[28] Liao, R.J., Tang, C., Yang, L.J., *et al.*: 'Thermal aging micro-scale analysis of power transformer pressboard', *IEEE Trans. Dielectr. Electr. Insul.*, 2008, **15**, (5), pp. 1281–1287

[29] Naranpanawe, L., Ekanayake, C., Saha, T.K.: 'Measurements on pressboard to understand the effect of solid insulation condition on monitoring of power transformer winding clamping pressure', *IET Sci. Meas. Technol.*, 2018, **13**, (2), pp. 186–192

[30] Linhjell, D., Lundgaard, L., Gäfvert, U.: 'Dielectric response of mineral oil impregnated cellulose and the impact of aging', *IEEE Trans. Dielectr. Electr. Insul.*, 2007, **14**, (1), pp. 156–169

[31] Bandara, K., Ekanayake, C., Saha, T.K.: 'Analysis of frequency domain dielectric response of pressboard insulation impregnated with different insulating liquids', *IEEE Trans. Dielectr. Electr. Insul.*, 2016, **23**, (4), pp. 2042–2050

[32] Cao Hongyan Birlasekaran, S.: 'Temperature dependent relaxation studies on oil-filled transformer'. Conf. Record of the the 2002 IEEE Int. Symp. on Electrical Insulation, Boston, USA, 2002, pp. 174–178

[33] Jonscher, A.K.: 'Dielectric relaxation in solids', *J. Phys. D. Appl. Phys.*, 1999, **32**, (14), p. R57

[34] El-Henawii, S.A., Saad, S.M., El-Answar, I.M.: 'Dielectric behavior of modified cellulose', *J. Mater. Sci. Technol.*, 1999, **15**, (2), pp. 164–168